Lattice dynamics and phase transitions in antifluorite crystals: K_2OsCl_6

Mark Sutton* and Robin L. Armstrong
Department of Physics, University of Toronto, Toronto, Ontario M5S 1A7, Canada

Brian M. Powell and William J. L. Buyers
Atomic Energy of Canada Limited, Chalk River Nuclear Laboratories, Chalk River, Ontario K0J 1J0, Canada
(Received 26 February 1982; revised manuscript received 27 September 1982)

Measurements of the inelastic neutron scattering from the antifluorite crystal K_2OsCl_6 are reported. Dispersion relations have been measured for the acoustic phonons in the cubic phase and for the acoustic and rotary phonons in the tetragonal phase. The rigid-ion model developed by O'Leary and Wheeler (OW) for antifluorite crystals cannot describe these results, particularly the low-frequency longitudinal-rotary mode which plays a major role in driving the phase transitions in certain antifluorite crystals. A simple extension of the OW model to include interactions between the potassium and osmium ions is found to overcome these difficulties. The inclusion of this interaction permits good agreement to be achieved for several optical frequencies and for the observed low-frequency rotary mode while simultaneously satisfying the equilibrium conditions. The new model provides a mechanism for the observed coupling of the order parameter and the elastic strains and suggests that elastic constant anomalies may be observed. The structural transitions in antifluorite crystals, which range from those involving ferro- or antiferro-rotative deformations with small attendant lattice distortions to those in which the lattice distortion predominates, appear to have a common origin in the softening of the longitudinal-rotary mode.

I. INTRODUCTION

From earlier neutron-diffraction measurements of the structure of the antifluorite crystal K_2OsCl_6,[1] it is known that a ferro-rotative transition occurs at $T_c = 44.5 \pm 0.4$ K. Subsequent inelastic neutron scattering measurements[2] showed that the longitudinal rotary mode at Γ softens and becomes unstable as T_c is approached from above. In the present paper additional inelastic neutron scattering results for some of the acoustic and rotary modes are reported in both the high-temperature cubic and low-temperature tetragonal phases.

In the isomorphous crystal K_2ReCl_6 a ferro-rotative transition occurs at 111 K followed by an antiferro-rotative transition at 103 K.[3] The transitions involve the softening of the longitudinal rotary branch of the dispersion relation at Γ and at X, respectively.[4] Since the frequency of the branch remains low along [001], and is almost independent of wave vector, it is clear that a delicate balance exists between the formation of long-range ferro-rotative and antiferro-rotative order in these antifluorite crystals.

A rigid-ion model was developed by O'Leary and Wheeler[3] (OW) to interpret the early spectroscopic data available for K_2ReCl_6. The model predicted a frequency for the zone-center rotary mode which was subsequently found to be too high by more than a factor of 2. The model has nonetheless been helpful in the interpretation of data for a variety of antifluorite crystals.[5,6]

Similarly, for K_2OsCl_6, the OW model cannot describe the phonon frequencies observed by inelastic neutron scattering. The purpose of the present work is not to provide a detailed lattice-dynamical model, but rather to provide increased understanding of the forces controlling the rotary-mode frequency, and to relate them to the qualitative changes in the lattice dynamics observed at the phase transition. In Sec. III we present an extension of the OW model and discuss the calculational procedures. The new model provides a good description of all available data for the cubic phase of K_2OsCl_6 and accounts for the changes which occur as a result of the phase transition.

In addition to structural transitions of the rotative type, transitions having the nature of a pure tetragonal distortion and transitions involving both a rotation and a lattice distortion have been identified in antifluorites.[7] Section IV contains comments on the relation between the qualitatively different types of transitions that have been observed.

II. NEUTRON INELASTIC SCATTERING EXPERIMENTS

Two single crystals[8] of K_2OsCl_6, with a total volume of ~ 2 cm^3, were studied at 7 K in the tetragonal phase and at 77 K in the cubic phase.

As the structure factor for the longitudinal-rotary mode is zero in high-symmetry planes[4] such as (110) and (001), the crystals were aligned so that the scattering plane was $(5\bar{3}0)$. The experiments were carried out with the N5 triple-axis spectrometer at the NRU reactor, Chalk River. The monochromator and analyzer were the germanium (111) and pyrolytic graphite (002) planes, respectively. The collimations were 0.6° and 0.7° before and after the specimen. The spectrometer was operated in the constant-$\vec{Q}$ mode with fixed analyzer energies E_1 of 2.6 or 3.0 THz, corresponding to frequency resolutions of 0.15 and 0.18 THz, respectively, for zero-frequency transfer.

Measurements were made along the [001] direction in the zones around (351) and (353). Structure-factor calculations indicated that both the longitudinal-rotary mode and the transverse-acoustic mode should be strong scatterers most of the way across the zone, and that the transverse-rotary mode should be strong near the zone center.[9] Figure 1 shows the peak that arises from the triply degenerate longitudinal- and transverse-rotary modes at the zone center.

Frequencies measured in the [001] direction are shown in Fig. 2. Calculated structure factors were used to identify the modes. The solid-line dispersion curves are those of the model described later. There is evidence for repulsion in the vicinity of (0,0,0.2) between the longitudinal-rotary (LR) and longitudinal-acoustic (LA) branches. This is expected as they have the same Δ_1 symmetry along [001] in the tetragonal phase.

Dispersion curves of the acoustic- and transverse-rotary modes at 77 K in the high-temperature cubic phase were measured with the crystals aligned in the $(1\bar{1}0)$ scattering plane. Data for the LR mode in this phase had been obtained previously[2] with crystal alignment in the $(5\bar{3}0)$ plane. The experiments were carried out on the L3 triple-axis spectrometer. The monochromator and analyzer were the germanium (113) and copper (002) planes, respectively. The collimations were 0.3° and 0.6° before and after the specimen. The spectrometer was operated in the constant-$\vec{Q}$ mode with a fixed analyzer energy E_1 of 8.25 THz. The frequency resolution was 0.45 THz for zero-energy transfer.

Measurements were made in the [100], [110], and [111] directions around several reciprocal-lattice points. The results are shown in Fig. 3 and are included in the tabulation in Sec. III. The solid-line dispersion curves are from the model described later. As expected from group theory, the longitudinal-acoustic modes are not coupled to the longitudinal-rotary modes.

III. RIGID-ION MODEL

Two rigid-ion models for antifluorite crystals have been discussed in the literature. The model introduced by O'Leary and Wheeler to calculate the dispersion curves for K_2ReCl_6 is based on forces between individual atoms. A second model proposed by Bates *et al.* for the discussion of hexamine nickel halides is based on interactions between rigid molecular units.[10] Since the latter crystals are of the form

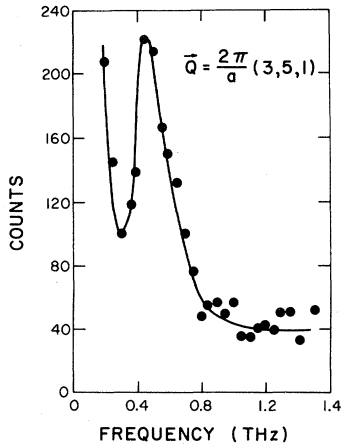

FIG. 1. Typical scan for a wave vector $(2\pi/a)(3,5,1)$. The peak is the rotary mode at the Γ point. The data were taken at 7 K. The line is a guide to the eye.

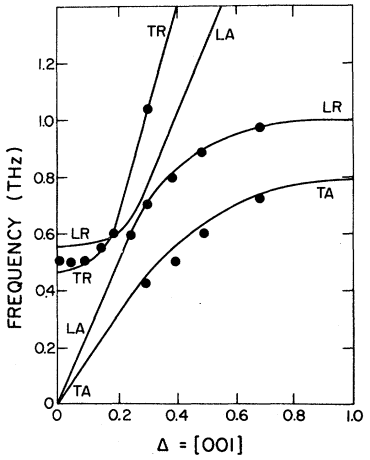

FIG. 2. Dispersion curves of the transverse- and longitudinal-rotary modes and the longitudinal-acoustic mode in the tetragonal phase at 7 K. The lines are from the model described in the text.

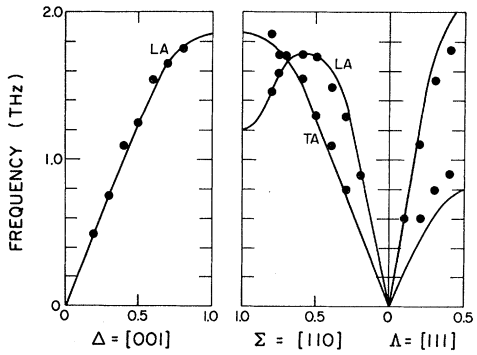

FIG. 3. Dispersion curves of the acoustic modes in the cubic phase along [001], [110], and [111] at 77 K. The lines are from a model fit.

NiY_6X_2, where $Y=NH_3$ and $X=Cl$, the model is also applicable to antifluorite crystals (R_2MX_6) which have an isomorphous crystal structure, but whose ionic structure is reversed, with the negative ion X replaced by the positive ion R.

The molecular model is not strictly applicable to K_2OsCl_6, since the internal molecular frequencies are not well separated from the external frequencies. Nonetheless, the model provides insight into the origin of translation-rotation coupling in the antifluorites. In an attempt to account for the failure of the OW model to predict the low frequency of the rotary mode, Bates *et al.*[10] claimed that the OW model neglects translation-rotation coupling. Their claim is based on the observation that within their molecular model, if the translation-rotation coupling is set to zero, the rotary modes are pure and not coupled to acoustic modes, as illustrated in Fig. 4(a).

When translation-rotation coupling is introduced, the set of coupled pseudorotary and pseudotranslational modes of Fig. 4(b) are produced. The main change is the different connectivity along Δ-X-Σ. The longitudinal-rotary branch remains flat along Δ because the transverse second-neighbor chlorine force constant is small.[2] Also, from group theory, these modes do not couple to LA modes.

In fact, the criticism of Bates *et al.* is invalid, as may be seen by starting from an atomic model and summing forces between atoms in different molecules. When this procedure is carried out for the OW model (see Appendix) a nonzero translation-rotation coupling results. Thus the suggestion of Bates *et al.* that the OW theory fails to account for the low rotary-mode frequency because it neglects translation-rotation coupling, is found to be incorrect. Although the difference between Fig. 4(a) and 4(b) is dramatic, it arises because a different connectivity of the branches through Δ-X-Σ has occured. Three possible connectivities are illustrated in Fig. 4. We find that the connectivity of our model [Fig. 4(c)] (and by implication that of the OW model) depends both on the frequency of the transverse-rotary (TR) and LR modes at Γ and also

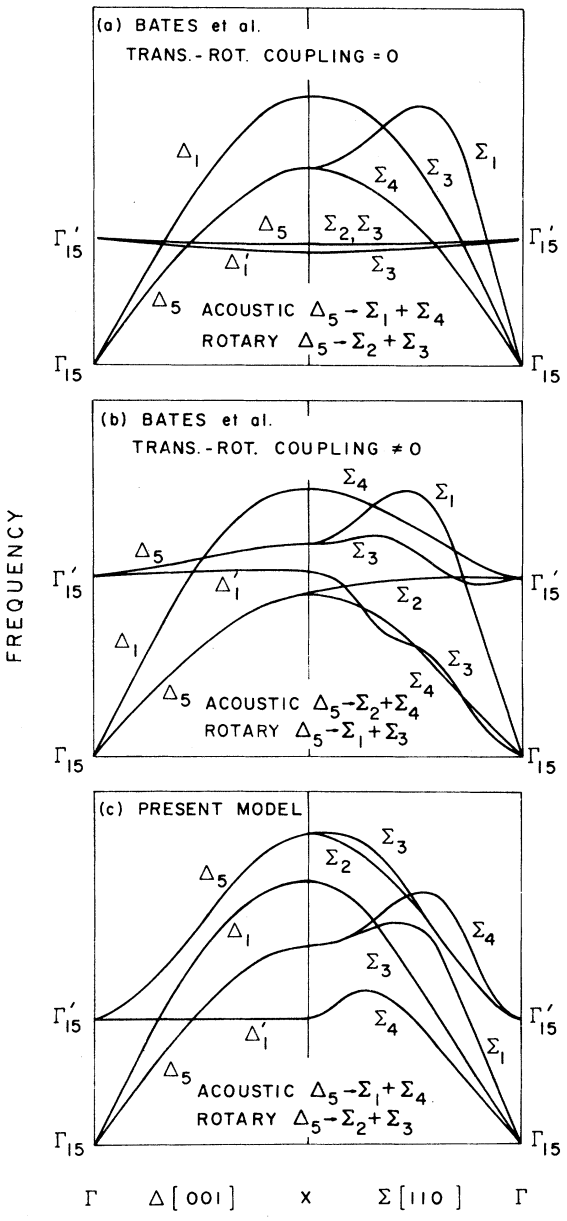

FIG. 4. Model dispersion curves for rotary and acoustic branches in cubic fluorite and antifluorite crystals. (a) Intermolecular translational-rotational coupling set to zero, (b) intermolecular translational-rotational coupling nonzero, and (c) present model with interatomic interactions.

TABLE I. Definition of the parameters used in the rigid-ion model. (See Fig. 5 for indexing scheme of bonds.)

O_h^5	C_{4h}^5
Charges	
q_K, q_{Os}, q_{Cl}	q_K, q_{Os}, q_{Cl}
Bonds[a]	
(1) Cl(2)-Cl(4) (0.5,0.5,0)[b]	(1) Cl(2) −Cl(4) (0.5,−0.5,0)
	(2) Cl(2) −Cl(4) (0.5,0,0.5)
	(3) Cl(6) −Cl(7) (0,−0.5,0.5)
	(6) Cl(2) −Cl(4) (0.5,0.5,0)
(2) K(8)-K(9) (0.5,0,0.5)	(4) K(8) −K(9) (0.5,0,0.5)
(3) Cl(2)-Cl(4)	(5) Cl(2) −Cl(4)
(4) Os(1)-K(8)	(7) Os(1) −K(8)
(5) Cl(2)-Cl(5) (0.5,0.5,0)	(8) Cl(2) −Cl(5) (0.5,0.5,0)
	(9) Cl(2) −Cl(7) (0.5,0,0.5,)
(6) Cl(2)-K(8)	(10) Cl(2) −K(8) (0,−0.5,−0.5)
	(11) Cl(6) −K(8) (−0.5,−0.5,0)
	(12) Cl(2) −K(8)
(7) Cl(2)-Cl(3)	(13) Cl(2) −Cl(3)
(8) Os(1)-Cl(2)	(14) Os(1)−Cl(2)
Number of constraints	
Charges 1	Charges 1
Forces 1	Forces 3
Stress 1	Stress 2
Independent parameters	
16	25

[a]Bonds are numbered in decreasing length.
[b]Atoms in unit cells other than the one at the origin are so indicated.

on the amount by which the TR frequency rises along Δ, thus affecting its interaction with the transverse-acoustic (TA), transverse-optic (TO), and transverse-lattice (TL) modes (see Figs. 6 and 8).

The interactions included in our modified OW model for both the cubic (O_h^5) and tetragonal (C_{4h}^5) phases are summarized in Table I and Fig. 5. To analyze the data, a set of programs was written to calculate dispersion curves for any crystal structure using a rigid-ion model. These programs were tested using the constants[3] of O'Leary and Wheeler to reproduce their results for K_2ReCl_6. The equilibrium conditions as given by Boyer and Hardy[11] were enforced. That is, the net force on each ion must be zero, as must the macroscopic stress tensor and the net charge per unit cell. These requirements give the number of constraints stated in Table I. The equilibrium conditions were imposed by considering the constraints as extra data and fitting them to zero. The procedure was verified by obtaining the results of Boyer and Hardy for the hexagonal crystal, wurtzite. To distinguish between modes as the calculation progressed, particularly the nearly degenerate TQ_4 and Q_5 modes, information on the eigenvectors was used.

A. Cubic phase

The data available[2,9,12] for the cubic phase fit are given in Table II. In addition, several modes have been measured[13] by vibronic spectroscopy in the tetragonal phase at 5 K. These are also listed in Table II. Noting that for the similar crystal K_2ReCl_6 little change was observed from room temperature to 4 K in the frequencies of any of the modes except the rotary-lattice mode, the vibronic data available for K_2OsCl_6 were also used for the cubic phase fit. The validity of this approximation is confirmed for the Q_2 and Q_4 modes by other spectroscopic data taken in the cubic phase.[12]

The model is sufficiently complicated that not all parameters could be varied simultaneously in the least-squares minimization procedure. Subsets of force constrants were selected and varied to bring specific calculated frequencies into agreement with the measured values. In order to execute the programs in the time available on the VAX computer

TABLE II. Spectroscopic data for K_2OsCl_6. All data, except that from vibronic spectroscopy, were measured for $T > T_c$. The vibronic data were taken at 5 K. Typical errors for the frequencies measured by inelastic neutron scattering are ±0.05 THz.

Mode	q	ν(THz) L	T	Type of measurement
A	(0,0,0.2)	0.5		Inelastic neutron[a]
A	(0,0,0.3)	0.75		
A	(0,0,0.4)	1.1		
A	(0,0,0.5)	1.25		
A	(0,0,0.6)	1.55		
A	(0,0,0.7)	1.65		
A	(0,0,0.8)	1.75		
A	(0,0.2,0.2)	0.9		
A	(0,0.3,0.3)	1.3	0.8	
A	(0,0.4,0.4)	1.5	1.1	
A	(0,0.5,0.5)	1.7	1.3	
A	(0,0.6,0.6)	1.7	1.55	
A	(0,0.7,0.7)	1.7	1.7	
A	(0,0.75,0.75)	1.6	1.7	
A	(0,0.8,0.8)	1.45	1.85	
A	(0.1,0.1,0.1)	0.6		
A	(0.2,0.2,0.2)	1.1	0.6	
A	(0.3,0.3,0.3)	1.55	0.8	
A	(0.4,0.4,0.4)	1.75	0.9	
R	(0,0,0.3)		1.35	
R	(0,0,0.4)		1.60	
R	(0,0,0.5)		1.75	
R	(0,0,0.8)		2.25	
R	(0,0,0)	0.68		Inelastic neutron[b]
R	(0,0,0.1)	0.65		
R	(0,0,0.2)	0.62		
R	(0,0,0.3)	0.68		
R	(0,0,0.4)	0.69		
R	(0,0,0.6)	0.72		
R	(0,0,0.9)	0.65		
R	(0,0,1)	0.67		
R	$(0.3,0.5,0)/\sqrt{34}$	0.7		
R	$(0.6,1.0,0)/\sqrt{34}$	0.75		
R	$(0.9,1.5,0)/\sqrt{34}$	0.95		
0	(0,0,0)	3.15	2.52	Vibronic[c]
0	(0,0,0.8)		2.65	Inelastic neutron[d]
0	(0,0,0.9)		2.60	Inelastic neutron[d]
Q_6	(0,0,0)	3.8	3.8	Vibronic[c]
Q_5	(0,0,0)	5.13	5.13	Vibronic[c]
Q_4	(0,0,0)	5.46	5.16	Vibronic,[c] Raman[e]
Q_3	(0,0,0)	9.68	9.68	Vibronic[c]
Q_2	(0,0,0)	9.47	9.47	Vibronic,[c] infrared[e]
Q_1	(0,0,0)	10.49	10.49	

[a]Present work, 77 K.
[b]Reference 2.
[c]Reference 13.
[d]Reference 9.
[e]Reference 12.

in Toronto, only the data at $\vec{q}=(0,0,0)$, $\vec{q}=(0,0,0.6)$, and $\vec{q}=(0,0.5,0.5)$ were used in the fitting. The quality of fit was essentially the same when other combinations of three wave vectors, including Γ, were used.

The main objective was to lower the frequency of the rotary mode, calculated with the OW model, so that it was in better agreement with observation.

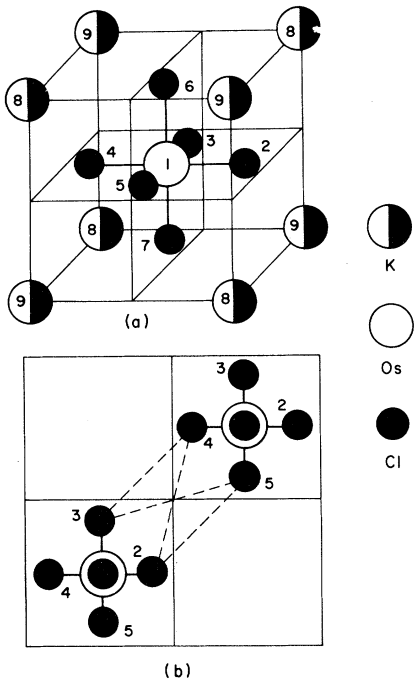

FIG. 5. Diagram to define the atomic numbering scheme used in Table I. (a) Local environment of an $OsCl_6$ octahedron, and (b) interoctahedral chlorine-chlorine couplings.

This caused the Q_5 mode to be too high in frequency while the longitudinal-optic (LO) modes were too low. The separation of these two modes could only be adjusted, within the OW model, if the equilibrium conditions (particularly stress equilibrium) were broken. The introduction of the additional bond Os—K allowed the rotary, Q_5, and LO modes to be simultaneously fitted while still maintaining equilibrium.

The final results are summarized in Table III and Figs. 3 and 6. The table lists the model parameters deduced from the fitting procedure and the figures show the calculated dispersion curves and all the measured spectroscopic data. It may be concluded that the model provides a good description of the available cubic-phase data except in the [111] direction. In particular, it is able to account for the absolute magnitude and the dispersion of the longitudinal- and transverse-rotary modes whereas the original OW model could not. Note the large splitting (Fig. 6) of the LR and TR modes along Δ.

As shown in Table III, the force constants of the present improved model differ from those of O'Leary and Wheeler in having an internal Cl-Cl xy radial force constant that is 3 times weaker, an external K-Cl radial force constant that is 50% stronger, and a long interoctahedral Cl-Cl radial force constant A_1, that is 4 times larger but of the opposite sign. O'Leary and Wheeler showed that the rotary-mode frequency could be lowered by a

TABLE III. Model parameters for K_2MCl_6 ($T > T_c$).

Bond[a] n	Bond length (Å)	Bond type	Force constants[b] ($N\,m^{-1}$) A_n OW[d]	A_n Present[c]	B_n OW[d]	B_n Present[c]
1	4.896	Cl—Cl (long inter)	0.67	−2.7±0.3	−1.5	0.006±0.0040
2	4.890	K—K	0.66	−1.2±0.6	0	3.4±0.3
3	4.652	Cl—Cl (intra xx)	31	30.8±0.2	−2.0	−5.6±0.5
4	4.235	M—K	0	0.6±0.4	0	−0.10±0.03
5	3.627	Cl—Cl (short inter)	6.3	5.8±0.2	0.27	−0.9±0.1
6	3.460	K—Cl	6.7	10.0±0.1	−1.1	−2.0±0.1
7	3.289	Cl—Cl (intra xy)	15	4.9±0.3	−2.7	−2.2±0.1
8	2.326	M—K	131	150.9±0.8	19	19.3±0.4

Ion	Charge (units of e)
K	0.77±0.05
Os	0.26±0.05
Cl	−0.30±0.01

[a]Bond numbering scheme as defined in Table I.

[b]$A_n=(\partial^2 V_n/\partial r^2)$, $B_n=(1/r_n)(\partial V_n/\partial)$, where V_n is the pair potential for bond n.

[c]Parameter values of present force model for K_2OsCl_6.

[d]Parameter values of the model of O'Leary and Wheeler for K_2ReCl_6.

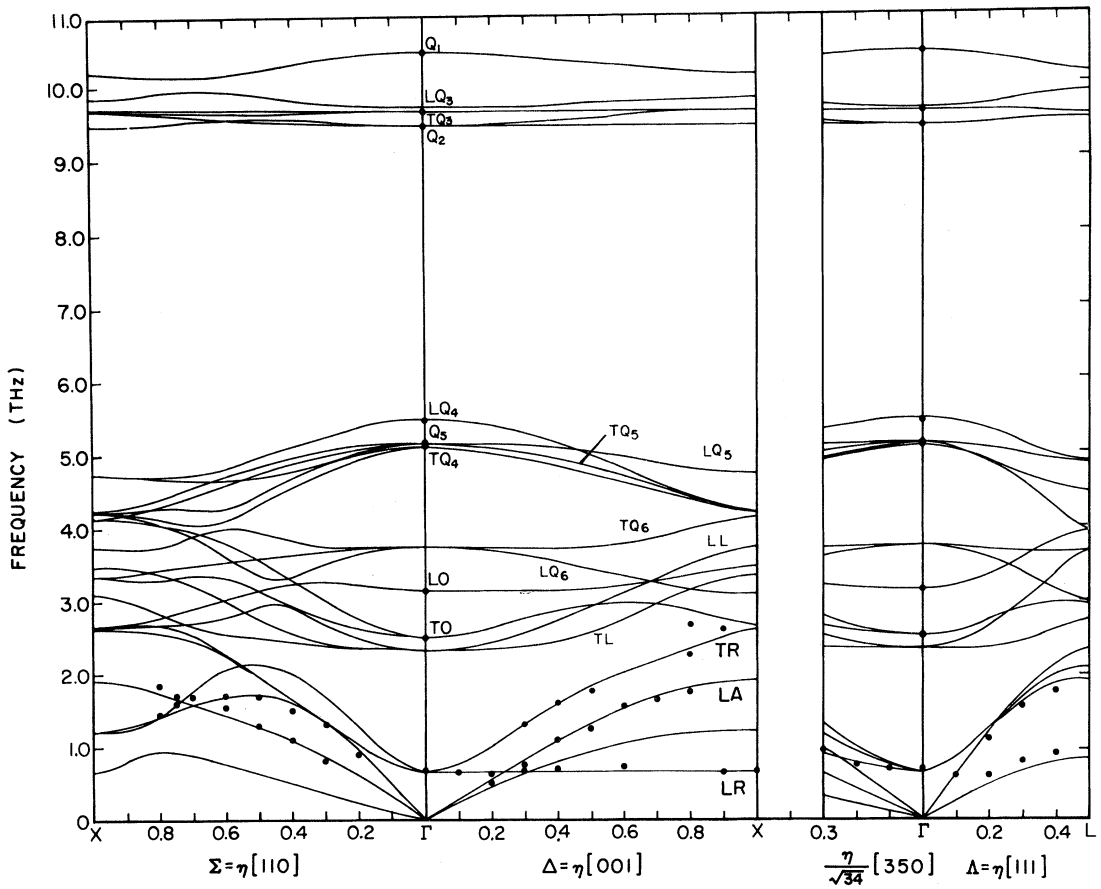

FIG. 6. Calculated dispersion curves for the cubic-phase rigid-ion model. All measured spectroscopic data are shown by points.

small decrease in A_1, but they did not investigate the possibility of a gross change in A_1. Although the present model gives a good account of the observed frequencies, and provides an interpolation scheme for K_2OsCl_6, we do not necessarily regard the fitted parameters as specifying realistic interatomic potentials.

The normal modes calculated at the Γ and X points were compared[14] with the molecular symmetry coordinates shown in Fig. 7. The comparison was instructive in that it showed the amount of mixing between the idealized internal and external modes and therefore illustrated the limitations of a molecular model for K_2OsCl_6. At the Γ point the rotary and optic modes are well-defined molecular modes. The internal normal modes are also very similar to the internal molecular modes, with the exception of Q_5. The two modes of symmetry T_{2g}, namely Q_5 and L, are strongly mixed. At the X point there is much more mode mixing. The only modes which retain their characters are the LR, LQ_6, and one of the Q_2 modes. This is because the LR mode has unique symmetry along [001] and the LQ_6 and Q_2 modes, which are the only two of their particular symmetry, are separated in energy by more than a factor of 3. The LA and LO modes have mixed so that the octahedra no longer move in the LO mode, and only the octahedra move in the LA mode. The longitudinal-lattice (LL) mode has become purely internal whereas the TQ_6 mode has become partly external in character.

B. Tetragonal phase

Considerably less spectroscopic data are available for the tetragonal phase. Only a few light-scattering results have been reported.[13] The neutron scattering data are those shown in Fig. 2 and were taken only along the [001] direction. As noted earlier, little change in the internal-mode frequencies is expected

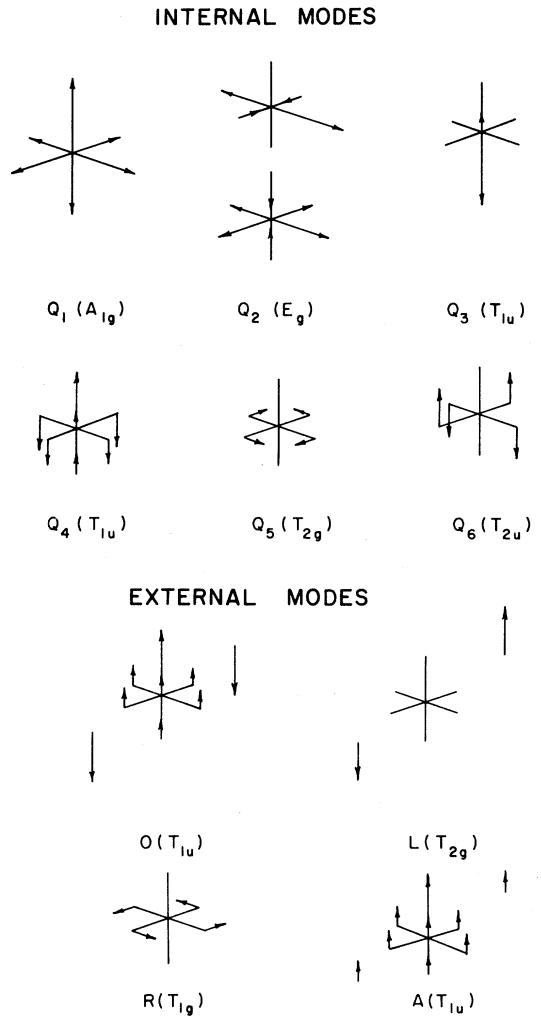

FIG. 7. Molecular-symmetry modes for a cubic antifluorite crystal.

as a result of the phase transition. Therefore, the optical data available for the cubic phase of K_2OsCl_6 were also used for the tetragonal phase. The neutron scattering data at wave vectors $\vec{q}=(0,0,0)$, $\vec{q}=(0,0,0.2)$, $\vec{q}=(0,0,0.3)$, and $\vec{q}=(0,0,0.5)$ used in the fitting were weighted more heavily than the optical data. To increase the number of constraints in the model, the charges on the ions were fixed at the values given by the cubic-phase fit.

The final results are summarized in Table IV and Figs. 2 and 8. The table lists the model parameters deduced from the fitting procedure and the figure shows the calculated dispersion curves and the neutron scattering data. In view of the larger number of adjustable parameters and the smaller number of

TABLE IV. Model parameters for K_2OsCl_6 ($T < T_c$).

Bond[a] n	Bond length (Å)	Force constants ($N\,m^{-1}$) A_n	B_n
1	5.141	−2.5	
2	4.858	−0.91	−0.28
3	4.848	−3.2	−0.51
4	4.845	−2.0	3.6
5	4.665	31.4	−5.6
6	4.556	−2.4	−0.3
7	4.196	0.32	0.37
8	3.566	7.7	0.07
9	3.560	4.4	0.12
10	3.532	10.0	−1.8
11	3.427	10.1	−0.20
12	3.325	10.2	−2.2
13	3.299	4.88	−2.4
14	2.332	151	20.1

[a]Bond numbering scheme is defined in Table I.

data, the fitting procedure based on varying subsets of parameters is far removed from a true least-squares fit; no errors are therefore quoted in Table IV. At best it might be expected qualitative agreement would be obtained, and this indeed is the case. In particular, the model is able to account for the LR-LA mode interaction along [001]. Interaction of the TO and TL modes is also expected from symmetry considerations. However, the rather large splittings of the LQ_4 and Q_6 modes at the Γ point are surprising. Whether or not these features are real should be checked in a future experiment. Nonetheless, the dispersion curves are very similar in the cubic and tetragonal phases and it may be concluded that the modified OW model is able to account for the dynamics of K_2OsCl_6 in both phases.

IV. DISCUSSION AND CONCLUSIONS

We have seen in Sec. III that a rigid-ion model gives a good description of the dispersion curves of K_2OsCl_6. The observation that in the cubic phase the LR branch is flat along [001] but rises rapidly in the [350] direction indicates that the motions of the $OsCl_6$ octahedra are highly correlated within x-y planes but weakly correlated between planes. In the model this correlation is determined by bond 1, the longest chlorine–chlorine interoctahedral bond. Mintz *et al.*[2] noted that the frequency $\omega(q_z)$ of the LR mode for a wave vector $(0,0,q_z)$ is given by

$$\begin{aligned} M_{\mathrm{Cl}}\omega^2(q_z) &= 4.21B_5+4A_1+2A_6+2.21B_6 \\ &\quad +4.42B_1+4B_1\sin^2(q_z a/4)+\cdots \\ &= 1.06+0.02\sin^2(q_z a/4)+\cdots , \end{aligned} \tag{1}$$

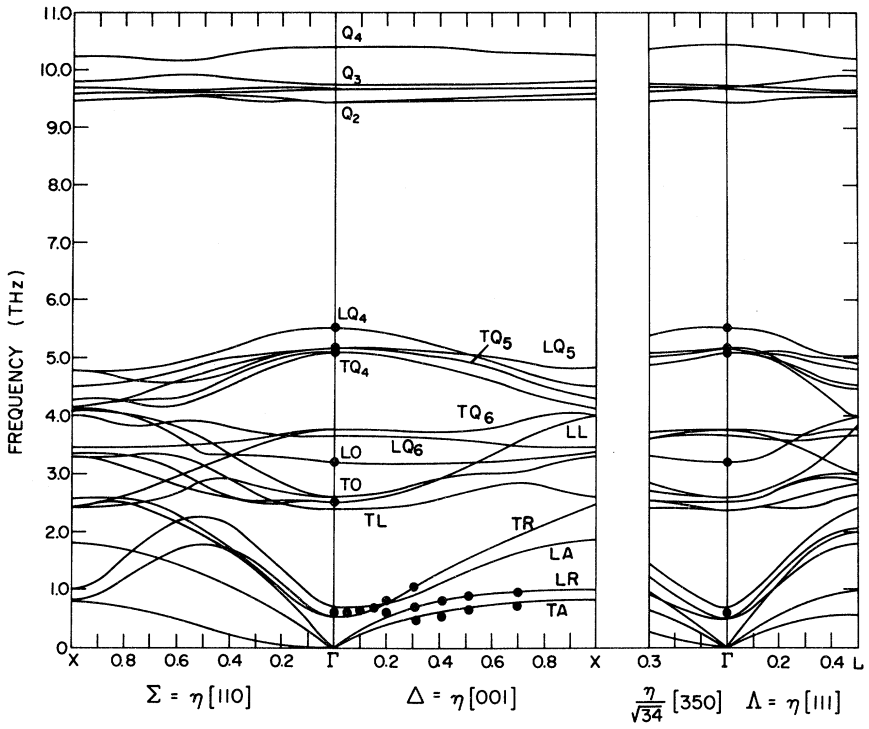

FIG. 8. Calculated dispersion curves for the tetragonal-phase rigid-ion model. All spectroscopic data used for the calculation are shown.

where the ellipsis stands for Coulomb terms and where M_{Cl} is the mass of a chlorine atom. Since the Coulomb term was shown to be small and almost independent of q_z, it was concluded from the weak correlation between x-y planes that B_1 must be small.[2] This prediction is confirmed by the present analysis which yields $B_1 = 0.006$, the smallest force constant in the model. The low frequency of the LR mode arises because of the near cancellation of oppositely contributing force constants; the first four terms in Eq. (1) contribute -3.75, -10.8, $+20.0$, and -4.42, respectively. Thus the strong repulsive short-range K-Cl radial force constant balances the sum of the attractive effects of the transverse part of the same force, the short interoctahedral Cl-Cl transverse force constant, and the long interoctahedral Cl-Cl radial force constant. Any of these four force constants can play a dominant role in the phase transition in antifluorites. In Table V we focus on the effect of the long interoctahedral radial force constant A_1, to show how sensitive the LR frequency is to the value of this force constant.

TABLE V. Relationship between $\nu_r(\Gamma)$ and the radial force constant A_1. Approximate temperatures are shown at which $\nu_r(\Gamma)$ was measured.

A_1 ($N\,m^{-1}$)	$\nu_r(\Gamma)$ (THz) Expt.	Calc.
−2.70	0.65(220 K)	0.66
−2.79	0.55(150 K)	0.53
−2.83	0.45(126 K)	0.46

The results were obtained by selecting three different values of $\nu_r(\Gamma)$ and letting only A_1 change in least-squares fits to all the frequencies. The values of A_1 and $\nu_r(\Gamma)$ deduced from the fits are given in the table. No other calculated frequencies changed significantly over this range of A_1.

Another important conclusion from the cubic-phase model relates to the connectivity of the rotary and acoustic branches as discussed earlier with reference to Fig. 4. Whereas for the OW model the rotary and acoustic branches are distinct, such is not the case for our modified model. The coupling of rotary and acoustic branches should mean that the order parameter of the phase transition is strongly coupled to the elastic strains and should produce a decrease in certain elastic constants near the phase transition. The observed thermal-expansion anomaly[15] near T_c might be explained by this type of coupling. The previous discussion of the anomaly[15] had

assumed that the elastic constants would not change significantly.

In the tetragonal phase the flatness of the LR mode along [001] is lost. A comparison of the force constants in the two phases shows that most of them remain close to their high-temperature values. Exceptions are those force constants associated with bond 1 of the cubic phase which becomes bonds 1,2,3,6 of the tetragonal phase. Since the behavior of the LR mode in the cubic phase is dominated by these Cl—Cl bond constants, it is not surprising that these parameters change as a result of the phase transition. The force constant B_1 shows the largest change in going from the cubic to the tetragonal phase and accounts for the increase in the dispersion of the LR mode along [001]. Physically this means that the two-dimensional nature of the correlations existing in the cubic phase is weaker in the tetragonal phase.

Finally, it is worthwhile to put the phase transition in K_2OsCl_6 into perspective with those in other antifluorite crystals. For example, K_2SnCl_6 undergoes a purely antiferro-rotative distortion[16] and Rb_2PtI_6 a purely tetragonal-lattice distortion.[7] The antiferro-rotative distortion in K_2SnCl_6 obviously depends on the rotary mode. However, the tetragonal distortion in Rb_2PtI_6 also involves the rotary mode, at least indirectly, as evidenced by the nuclear-quadrupole-resonance spin-lattice relaxation data.[17,18] Further evidence of the relation between transitions which exhibit tetragonal distortions and those which show rotative deformations is given by measurements of elastic constants.[19,20] For both K_2SnCl_6 and K_2ReCl_6 the elastic constant $C_{11}-C_{12}$ decreases dramatically near the phase transition; this is the elastic constant that governs the tetragonal distortion[21] in Rb_2PtI_6. Note also that this constant gives the velocity of the T_2A [110] mode, and it is this mode which connects to the LR mode at the X point. It would seem reasonable, therefore, to suggest that both rotative and tetragonal distortions can be explained by a softening of the LR mode. This mode, since it is so flat, can go soft at either the Γ or the X point. Because of its connectivity to the TA mode along [110], the order parameter for the rotative distortion must be coupled to the elastic strains. This coupling can lead to a phase transition which is first order as in K_2SnCl_6, to a phase transition which involves only a tetragonal distortion as in Rb_2PtI_6 or to a phase transition which involves both an antiferro-rotation and a tetragonal distortion[7] as in $(NH_4)_2PtI_6$.

ACKNOWLEDGMENTS

We are grateful for the expert technical assistance of H. F. Nieman, D. C. Tennant, and M. M. Potter.

APPENDIX: RELATIONSHIP BETWEEN ATOMIC AND MOLECULAR RIGID-ION MODELS

This appendix is based on the discussion given by Venkataraman and Sahni.[22] For a rigid molecule, whose atoms are at positions $\vec{x}(\kappa)$ away from the center of mass the rotation-translation force-constant tensor $\underline{\Phi}^{rt}$ can be expressed as a summation over the interatomic force constants as

$$\underline{\Phi}^{rt}\begin{bmatrix} l & l' \\ n & n' \end{bmatrix} = -\sum_{\kappa\kappa'} \vec{x}(\kappa)\cdot\underline{\Phi}\begin{bmatrix} l & l' \\ n & n' \\ \kappa & \kappa' \end{bmatrix} .$$

To prove that the atomic rigid-ion model of OW includes a rotation-translation coupling, we need only calculate the coupling of a translation of one of the R ions in the R_2MX_6 unit cell to a rotation of the MX_6 molecule. In the model there are only three such bonds of length r (Fig. 5) to consider—the bonds between the K(8) ion at $(\frac{1}{4},\frac{1}{4},\frac{1}{4})$ and the Cl ions at Cl(2)$=(u,0,0)$, Cl(3)$=(0,u,0)$, and Cl(6)$=(0,0,u)$, for which the force tensor has the schematic form

$$\underline{\Phi}\begin{bmatrix} 0 & 0 \\ 2 & 8 \end{bmatrix} = \begin{bmatrix} a & b & b \\ b & c & d \\ b & d & c \end{bmatrix} .$$

The other force-constant matrices are obtained by symmetry to give a total contribution

$$\underline{\Phi}^{rt} = u(b-c)\begin{bmatrix} 0 & 1 & -1 \\ -1 & 0 & 1 \\ 1 & -1 & 0 \end{bmatrix} ,$$

where

$$b = \frac{(A_6-B_6)\delta}{4r^2}$$

and

$$c = \left[\frac{(A_6+B_6)}{16} + B_6\delta^2\right]\Big/ r^2 ,$$

where $\delta = 1/4-u$. This is obviously not zero in general and shows explicitly the coupling of the rotations of the MX_6 octahedra to the translations of the R ions.

*Present address: Department of Physics, Massachusetts Institute of Technology, Cambridge, MA 02139.

[1]R. L. Armstrong, D. Mintz, B. M. Powell, and W. J. L. Buyers, Phys. Rev. B 17, 1260 (1978).

[2]D. Mintz, R. L. Armstrong, B. M. Powell, and W. J. L. Buyers, Phys. Rev. B 19, 448 (1979). See also D. Mintz, Ph.D. thesis, University of Toronto, 1978 (unpublished).

[3]G. P. O'Leary and R. G. Wheeler, Phys. Rev. B 1, 4409 (1970).

[4]J. W. Lynn, H. H. Patterson, G. Shirane, and R. G. Wheeler, Solid State Commun. 27, 859 (1978).

[5]S. Chodos and R. Berg, J. Chem. Phys. 70, 4864 (1979).

[6]H. H. Patterson and J. W. Lynn, Phys. Rev. B 19, 1213 (1979).

[7]M. Sutton, R. L. Armstrong, B. M. Powell, and W. J. L. Buyers, Can. J. Phys. 59, 449 (1981).

[8]Crystals were grown by S. Mroczkowski of Yale University.

[9]In the cubic phase, only the LR mode was predicted to scatter appreciably.

[10]A. R. Bates, I. L. A. Crick, and R. O. Davies, J. Phys. C 9, 3013 (1976).

[11]L. L. Boyer and J. R. Hardy, Phys. Rev. B 7, 2886 (1973).

[12]M. Debeau and H. Poulet, Spectrochim. Acta 25A, 1553 (1969).

[13]D. F. Durocher and P. B. Dorain, J. Chem. Phys. 61, 1361 (1974).

[14]The eigenvectors of the normal modes are displayed explicitly in the Ph.D. thesis of M. Sutton, University of Toronto, 1981 (unpublished).

[15]H. W. Willemsen, C. A. Martin, P. P. M. Meincke, and R. L. Armstrong, Phys. Rev. B 16, 2283 (1977).

[16]H. Boysen and A. W. Hewat, Acta Crystallogr. Sect. B 34, 1412 (1978).

[17]R. G. C. McElroy and R. L. Armstrong, Phys. Rev. B 18, 1352 (1978).

[18]H. M. van Driel and R. L. Armstrong, Can. J. Phys. 53, 1141 (1975); 54, 1087 (1976).

[19]W. Henkel, J. Pelzl, K. H. Hock, and H. Thomas, Z. Phys. B 37, 321 (1980).

[20]J. Pelzl, K. H. Hock, A. J. Miller, P. J. Ford, and G. A. Saunders, Z. Phys. B 39, 329 (1981).

[21]R. A. Cowley, Adv. Phys. 29, 1 (1980).

[22]G. Venkataraman and V. C. Sahni, Rev. Mod. Phys. 42, 409 (1970).